DOI: 10.1002/chem.200601568

# Copper(II) Interaction with Prion Peptide Fragments Encompassing Histidine Residues Within and Outside the Octarepeat Domain: Speciation, Stability Constants and Binding Details

**Katalin Ősz,[a] Zoltán Nagy,[a] Giuseppe Pappalardo,[b] Giuseppe Di Natale,[c] Daniele Sanna,[d] Giovanni Micera,[e] Enrico Rizzarelli,*[c] and Imre Sóvágó*[a]**

**Abstract:** A 31-mer polypeptide, which encompasses residues 84–114 of human prion protein HuPrP(84–114) and contains three histidyl residues, namely one from the octarepeat (His85) and two histidyl residues from outside the octarepeat region (His96 and His111), and its mutants with two histidyl residues HuPrP(84–114)His85Ala, HuPrP-(84–114) His96Ala, HuPrP(84–114)-His111Ala and HuPrP(91–115) have been synthesised and their $Cu^{2+}$ complexes studied by potentiometric and spectroscopic (UV/Vis, CD, EPR, ESI-MS) techniques. The results revealed a high $Cu^{2+}$-binding affinity of all peptides, and the spectroscopic studies made it possible to clarify the coordination mode of the peptides in the different complex species. The imidazole nitrogen donor atoms of histidyl residues are the exclusive metal-binding sites below pH 5.5, and they have a preference for macrochelate structure formation. The deprotonation and metal-ion coordination of amide functions take place by increasing the pH; all of the histidines can be considered to be independent metal-binding sites in these species. As a consequence, di- and trinuclear complexes can be present even in equimolar samples of the metal ion and peptides, but the ratios of polynuclear species do not exceed the statistically expected ones; this excludes the possibility of cooperative $Cu^{2+}$ binding. The species with a ($N_{im}$,N,N)-binding mode are favoured around pH 7, and their stability is enhanced by the macrochelation from another histidyl residue in the mononuclear complexes. The independence of the histidyl sites results in the existence of coordination isomers and the preference for metal binding follows the order of: His111 > His96 > His85. Deprotonation and metal-ion coordination of the third amide functions were detected in slightly alkaline solutions at each of the metal-binding sites; all had a ($N_{im}$,N,N,N)-coordination mode. Spectroscopic measurements also made it clear that the four lysyl amino groups of the peptides are not metal-binding sites in any cases.

**Keywords:** circular dichroism · coordination modes · copper · EPR spectroscopy · human prion protein · peptides

[a] Dr. K. Ősz, Dr. Z. Nagy, Prof. I. Sóvágó
Department of Inorganic and Analytical Chemistry
University of Debrecen, 4010 Debrecen (Hungary)
Fax: (+36) 52-489-667
E-mail: sovago@delfin.unideb.hu

[b] Dr. G. Pappalardo
CNR Institute of Biostructures and Bioimaging
V.le A. Doria, 95125 Catania (Italy)

[c] Dr. G. Di Natale, Prof. E. Rizzarelli
Department of Chemical Sciences, University of Catania
V.le A. Doria 6, 95125 Catania (Italy)
Fax: (+39) 095-337-678
E-mail: erizzarelli@unict.it

[d] Dr. D. Sanna
CNR Institute of Biomolecular Chemistry
Traverse La Crucca 3, 07040 Baldinca-Li Punti (SS) (Italy)

[e] Prof. G. Micera
Department of Chemistry, University of Sassari
Via Vienna 2, 07100 of Sassari (Italy)

Supporting information for this article is available on the WWW under http://www.chemeurj.org/ or from the author.

## Introduction

Prion diseases are a group of neurodegenerative pathologies that include Creutzfeldt–Jakob disease in humans, scrapie in sheep, and bovine spongiform encephalopathy in cattle.[1,2] They represent a peculiar case in biology due to the now widely accepted "protein only" hypothesis, which is based on the conformational conversion of the normal protein, $PrP^{C}$, to the disease-related isoform $PrP^{Sc}$.[3]

Mammalian $PrP^{C}$ is a 209-residue polypeptide that is anchored to the cell membrane through a glycosylphosphatidylinositol moiety. It comprises a flexible and a disordered N-terminal domain,[4] and a globular, mainly α-helical C-terminal domain.[5] This glycoprotein is most abundant in the central nervous and immune systems, but it is also expressed in other biological compartments.[6] The physiological function of PrP has not been identified unambiguously yet,[7,8] but increasing evidence indicates that it is a copper-binding

  

protein.[9–23] Residues 60–91 of the $PrP^C$ protein comprise four tandem repeats with the consensus sequence PHGGGWGQ. It is this region, known as the octapeptide repeats, that was first discovered to bind $Cu^{2+}$,[10,11] and, since then, considerable work has been devoted to identify the number of binding sites, their affinities and the coordination environment for both the octapeptide repeats and the full-length prion protein.[9,12–23] Until recently, the accepted model of $Cu^{2+}$ binding to the full-length prion protein, at pH 7.4, invoked six $Cu^{2+}$ ions bound at different sites: one metal ion can be accommodated in each of the four octapeptide repeats, and the remaining ions coordinate at two copper-ion sites that involve the His96 and His111 residues; each of these involves a single histidine imidazole and amide nitrogen atoms from nearby amino acid residues. However, new results indicate that at unsaturated $Cu^{2+}$ occupancy, copper coordination by the octapeptide repeats is different from the saturated occupancy state. Furthermore, it has been shown that the model described above provides an incomplete description of $Cu^{2+}$ binding in the prion protein. For instance, it has been demonstrated that a peptide representing the four octapeptide repeats displays multiple modes of $Cu^{2+}$ binding at pH 7.4.[24–26] Most of the data indicate that the affinity of PrP for $Cu^{2+}$ is in the low micromolar range,[14,15,20,21] but higher affinity values, that is, in the femtomolar range, have also been reported.[12]

Peptides that represent the octapeptide repeats, however, cannot be considered to be a complete model for $Cu^{2+}$ binding to the prion protein. Copper(II)-binding sites within the N terminus, but outside the octapeptide repeats have also been indicated; these involve His96 and His111.[12,19,27–30] It has also been suggested that this further $Cu^{2+}$-binding site has a higher affinity for $Cu^{2+}$ than the octameric repeat region.[12,27] The literature data on the complex-forming ability of histidyl residues outside the octarepeat domain are rather contradictory. Among them, His96 and His111 are in the unordered region of the protein. An EPR study suggested that only His96 is the locus for $Cu^{2+}$ coordination,[16,19] while EXAFS, CD, EPR, and NMR spectroscopy studies implicated His111, Met109/112, and His96 to be the coordinating amino acids.[31,32] A more recent study reconsidered previously published data and indicated that $Cu^{2+}$ independently binds to residues His96 or His111.[28] A thermodynamic and structural study has been performed on the $Cu^{2+}$ complexes of HuPrP(106–126). However, an N-terminal free peptide was used in this study, and the results revealed a preference at the coordination of the N terminus that is not possible under biological conditions.[33]

Most recent publications from our laboratories have contributed towards a better understanding of the metal-binding ability of histidyl residues outside the octarepeat domain.[29,34,35] Copper(II) complexes of tetra-, penta- and nonapeptide fragments of HuPrP including His96, His111 and His187 residues have been studied by the combined applications of potentiometric and the most common spectroscopic techniques, including UV/Vis, CD, EPR, and NMR spectroscopy. Histidyl imidazole N-donor atoms were found to be the primary $Cu^{2+}$ binding sites in all peptides, and the preference for the formation of 3N- and 4N-complexes that contain an additional two or three deprotonated amide functions was suggested around the physiological pH range. The difference in the sizes of the fused chelate rings resulted in the enhanced metal-binding affinity of the peptide fragments, including His96 or His111 (six-membered chelate) compared to that of a single octarepeat monomer (seven-membered chelate). It is thus clear that for a full understanding of $Cu^{2+}$ binding to the prion protein, the relative affinity of these sites needs to be investigated. Unfortunately, the full-length prion protein is poorly soluble above pH 6,[19,20] and the concentration range that is needed to obtain reliable $Cu^{2+}$-affinity constants by potentiometric titrations is higher than the commonly used μM concentrations. On the other hand, it also should be considered that the preference for binding to the histidyl residue outside the octarepeat domain was determined only for short fragments. Thus, to study the involvement of multiple histidine–$Cu^{2+}$ coordination, soluble polypeptide fragments of prion N-terminus-encompassing histidine residues, within and outside the octarepeat domain, are the best candidates to obtain the speciation at different pH values, and various metal-to-protein ratios, as well as reliable affinity constants for the $Cu^{2+}$ species. In this context, we report here the synthesis and the stability constants of the $Cu^{2+}$ complexes with the 31-mer polypeptide that encompasses the residues 84–114 of human PrP, that is, HuPrP(84–114); this peptide contains three histidine residues, namely one from the octarepeat (His85), and two histidine residues from outside the octarepeat region (His96 and His111). To obtain a detailed description of the peptides' protonation constants and their $Cu^{2+}$-complex speciations, a series of potentiometric measurements in the pH 3–11 range and at different metal-to-ligand ratios have been carried out. These were coupled with the ESI-MS measurements, which aided the interpretation of the equilibria data by confirming the stoichiometry of the metal complex formed. In addition, we used UV/Vis and EPR spectroscopy to get complementary information about the number of coordinated nitrogen atoms as well as the geometry of the $Cu^{2+}$ complexes; CD spectra helped us to differentiate between the different types of nitrogen atoms that participate in metal coordination. The comparison of the equilibrium and spectroscopic data between the HuPrP(84–114) with its mutants HuPrP(84–114)His85Ala, HuPrP(84–114)His96Ala, HuPrP(84–114)His111Ala and HuPrP(91–115) made it possible to evaluate the metal-binding affinity of the three-histidine-containing peptide HuPrP(84–114) and its two-histidine mutants, which makes a much more reliable model to understand the metal-binding ability of the native protein.

## Results and Discussion

**Protonation of the ligands**: Protonation constants of the peptide fragments of human prion protein have been deter-

  

mined by potentiometric titrations, and the data are included in Table 1. All peptides include the amino acids between 91 and 114, in which four lysyl residues are located at the Lys101, Lys104, Lys106 and Lys110 positions. In addition, the molecules contain two or three histidyl residues, namely His85, His96 and His111 for HuPrP(84–114), His96 and His111 for HuPrP(84–114)His85Ala and HuPrP(91–115), His85 and His111 for HuPrP(84–114)His96Ala and His85 and His96 for HuPrP(84–114)His111Ala.

In agreement with the primary sequence, seven or six p$K$ values can be calculated for the peptides, and these values are also listed in Table 1. Even the overall stability constants of the protonated species from $[HL]^+$ to $[H_7L]^{7+}$ show high similarity between the values, but this is especially clear from the stepwise p$K$ values. From the previous studies on small peptide fragments[29,34] it is evident that the high p$K$ values (in the range from 9.26 to 10.68) can be assigned to the deprotonation of the lysyl ammonium groups. The average values for these deprotonation reactions are between 10.05 and 10.09, and this range is comparable to the error in the data. Deprotonations of the four lysyl residues take place in overlapping processes, and none of the p$K(Lys_{1-4})$ values can be assigned to any specific amino acids in the sequence. The same parallel deprotonation of the lysyl side chains was reported to occur in the smaller nonapeptide fragments HuPrP(106–114), which contain only two lysyl residues.[29]

Deprotonations of the protonated imidazolium side chains take place in the pH range from 5 to 7, with the average values changing from 6.18 to 6.28. The small differences in the p$K$ values of the five ligands suggest that the deprotonation of the imidazolium groups also completely overlaps. As a consequence, the stepwise constants cannot be assigned to specific histidyl residues and all data can only be considered to be simple macroscopic thermodynamic parameters. A detailed pH–NMR titration of the peptides by using various 2D NMR spectroscopy techniques might provide some information on the individual protonation sites of the ligands. This work is in progress in our laboratories, and the results will be presented in a forthcoming publication.

**Equilibria analysis of the $Cu^{2+}$ complexes**: The stability constants of the $Cu^{2+}$ complexes of all peptides have been determined by potentiometric titrations by using three different metal-to-ligand ratios (M/L 3:1, 2:1, and 1:1) for all of the investigated PrP fragments. In the $Cu^{2+}$–HuPrP(84–114) system, the precipitation of copper(II) hydroxide was never observed at any M/L ratios or pH values; this suggests the formation of mono-, bi-, and trinuclear complexes. In the case of the mutants that contain only two histidyl residues, precipitation of copper(II) hydroxide occurred in the 3:1 M/L ratio samples above pH 6.5, and it would not dissolve even at high pH values. These observations indicate that the number of $Cu^{2+}$ ions that are bonded by the peptides is equal to the number of histidyl residues that are present in the molecules. The stability constants of 34 different species can be calculated in the $Cu^{2+}$–HuPrP(84–114) system (see Table 2), but it requires the use of the HYPERQUAD computer program.[36] All possible spectroscopic techniques that can be applied for paramagnetic $Cu^{2+}$ complexes, including UV/Vis, CD and EPR spectroscopy and MS, were used to check and/or modify the computational models. Selective line-broadening of $^1$H NMR spectra of $Cu^{2+}$ complexes have been frequently used to indicate the location of metal-binding sites.[37] In our case, however, due to the presence of coordination isomers at all ratios and all pH values, the application of this technique was not possible. All spectroscopic data (discussed below) suggest that the imidazole residues of the peptides behave as independent metal-binding sites, and the coordination modes of the short peptide fragments reported for the octarepeat monomer,[38] for HuPrP(94–97),[34] and for HuPrP(106–114)[29] can be used as the starting points for the development of the computational model. The best fitting of the potentiometric data was obtained by invoking the species listed in Table 2, and the corresponding speciation curves at two different metal-to-ligand ratios are plotted in Figure 1. The solid lines in Figure 1 show the concentrations of individual species, while the overall concentrations of mono-, di-, and trinuclear complexes are indicated by dotted lines. The reproducibility of the models reported in Table 2 was checked by parallel titrations of the sys-

Table 1. Protonation constants for the peptide fragments of prion protein ($T = 298$ K, $I = 0.2$ mol dm$^{-3}$ KCl, standard deviations are in parentheses).

| Species | HuPrP(84–114) | HuPrP(91–115) | HuPrP(84–114)His85Ala | HuPrP(84–114)His96Ala | HuPrP(84–114)His111Ala |
|---|---|---|---|---|---|
| $[HL]^+$ | 10.68(3) | 10.68(2) | 10.65(2) | 10.65(2) | 10.66(3) |
| $[H_2L]^{2+}$ | 20.96(2) | 20.95(3) | 21.06(3) | 21.01(2) | 20.96(2) |
| $[H_3L]^{3+}$ | 30.94(2) | 30.93(3) | 31.04(2) | 30.99(2) | 30.95(2) |
| $[H_4L]^{4+}$ | 40.22(1) | 40.19(2) | 40.35(2) | 40.32(2) | 40.30(2) |
| $[H_5L]^{5+}$ | 46.99(2) | 46.76(2) | 46.94(2) | 46.87(3) | 46.97(3) |
| $[H_6L]^{6+}$ | 53.18(3) | 52.54(2) | 52.72(2) | 52.64(2) | 52.85(2) |
| $[H_7L]^{7+}$ | 58.82(2) | – | – | – | – |
| p$K(Lys_1)$ | 10.68 | 10.68 | 10.65 | 10.65 | 10.66 |
| p$K(Lys_2)$ | 10.28 | 10.27 | 10.41 | 10.36 | 10.30 |
| p$K(Lys_3)$ | 9.98 | 9.98 | 9.98 | 9.98 | 9.99 |
| p$K(Lys_4)$ | 9.28 | 9.26 | 9.31 | 9.33 | 9.35 |
| p$K(His_1)$ | 6.77 | 6.57 | 6.59 | 6.55 | 6.67 |
| p$K(His_2)$ | 6.19 | 5.78 | 5.78 | 5.77 | 5.88 |
| p$K(His_3)$ | 5.64 | – | – | – | – |
| p$K(Lys)_{average}$ | 10.06 | 10.05 | 10.09 | 10.08 | 10.08 |
| p$K(His)_{average}$ | 6.20 | 6.18 | 6.19 | 6.16 | 6.28 |

  

Table 2. Stability constants for the $Cu^{2+}$ complexes of peptide fragments of prion protein ($T=298$ K, $I=0.2$ mol dm$^{-3}$ KCl, standard deviations are in parentheses).

| Species | HuPrP(84–114) | HuPrP(91–115) | HuPrP(84–114)His85Ala | HuPrP(84–114)His96Ala | HuPrP(84–114)His111Ala |
|---|---|---|---|---|---|
| mononuclear complexes | | | | | |
| $[CuH_6L]^{8+}$ | 57.51(3) | – | – | – | – |
| $[CuH_5L]^{7+}$ | 52.20(4) | 50.78(3) | 50.48(5) | 50.58(4) | 51.40(3) |
| $[CuH_4L]^{6+}$ | 46.69(3) | 45.02(4) | 44.90(4) | 45.03(5) | 45.90(3) |
| $[CuH_3L]^{5+}$ | 40.13(4) | 39.10(5) | 38.97(4) | 39.14(5) | 39.65(3) |
| $[CuH_2L]^{4+}$ | 33.44(2) | 32.81(3) | 32.84(3) | 32.44(3) | 32.67(3) |
| $[CuHL]^{3+}$ | 25.45(2) | 25.05(2) | 25.30(2) | 24.47(3) | 24.20(3) |
| $[CuL]^{2+}$ | 16.24(3) | 15.79(2) | 16.04(2) | 14.93(4) | 14.59(4) |
| $[CuH_{-1}L]^{+}$ | 6.50(3) | 5.81(3) | 6.08(2) | 4.96(4) | 4.68(4) |
| $[CuH_{-2}L]$ | −3.92(4) | −4.58(4) | −4.25(4) | −5.63(5) | −5.60(5) |
| $[CuH_{-3}L]^{-}$ | −14.62(6) | −15.20(7) | −14.88(6) | −16.35(6) | −16.23(8) |
| $[CuH_{-4}L]^{2-}$ | −25.65(10) | – | – | −27.43(12) | −27.32(10) |
| dinuclear complexes | | | | | |
| $[Cu_2H_3L]^{7+}$ | 44.28(10) | – | – | – | – |
| $[Cu_2H_2L]^{6+}$ | 38.21(8) | 36.56(8) | 35.71(7) | 35.62(8) | 36.95(6) |
| $[Cu_2HL]^{5+}$ | 31.77(7) | 30.55(7) | 30.00(7) | 30.01(6) | 30.56(7) |
| $[Cu_2L]^{4+}$ | 24.95(4) | 24.31(4) | 24.07(4) | 23.68(5) | 23.92(4) |
| $[Cu_2H_{-1}L]^{3+}$ | 17.35(3) | 17.02(3) | 16.78(4) | 16.15(4) | 16.06(4) |
| $[Cu_2H_{-2}L]^{2+}$ | 9.17(4) | 8.90(4) | 8.89(4) | 7.41(5) | 6.93(5) |
| $[Cu_2H_{-3}L]^{+}$ | 0.17(5) | −0.65(6) | −0.63(5) | −1.98(7) | −2.53(7) |
| $[Cu_2H_{-4}L]$ | −9.72(6) | −10.63(6) | −10.57(7) | −12.00(7) | −12.59(7) |
| $[Cu_2H_{-5}L]^{-}$ | −19.97(6) | −21.07(7) | −20.99(6) | −22.22(8) | −22.86(8) |
| $[Cu_2H_{-6}L]^{2-}$ | −30.59(8) | −31.71(9) | −31.66(10) | −32.82(8) | −33.53(10) |
| $[Cu_2H_{-7}L]^{7-}$ | −41.66(10) | – | – | −43.63(14) | −44.66(15) |
| trinuclear complexes | | | | | |
| $[Cu_3L]^{6+}$ | 28.78(10) | – | – | – | – |
| $[Cu_3H_{-1}L]^{5+}$ | 22.36(8) | – | – | – | – |
| $[Cu_3H_{-2}L]^{4+}$ | 15.59(7) | – | – | – | – |
| $[Cu_3H_{-3}L]^{3+}$ | 8.50(5) | – | – | – | – |
| $[Cu_3H_{-4}L]^{2+}$ | 0.40(6) | – | – | – | – |
| $[Cu_3H_{-5}L]^{+}$ | −8.25(7) | – | – | – | – |
| $[Cu_3H_{-6}L]$ | −17.55(8) | – | – | – | – |
| $[Cu_3H_{-7}L]^{-}$ | −27.51(9) | – | – | – | – |
| $[Cu_3H_{-8}L]^{2-}$ | −37.89(10) | – | – | – | – |
| $[Cu_3H_{-9}L]^{3-}$ | −48.54(12) | – | – | – | – |
| $[Cu_3H_{-10}L]^{4-}$ | −59.45(14) | – | – | – | – |

tems, and by computer evaluations of the data, and more importantly, these models and the corresponding speciation curves are in a good agreement with the spectroscopic measurements.

Before discussing the structural characterisation of the various species, some general comments related to the equilibria parameters should be considered. It is evident from Table 2 that both mono- and polynuclear species can exist in different protonation stages, mainly caused by the presence of the four lysyl residues in all peptides. Spectroscopic data, in agreement with the previous results on the short fragments, definitely prove that the amino groups of the lysines are not metal-binding sites at any pH values, and their deprotonation reaction takes place in the same pH range as reported for the free ligands (above pH 9). As a consequence, the overall stoichiometries of all species that exist below pH 9 contain four ammonium groups from lysines and their proton contents have to be taken into account to understand the binding modes of various species, that is, $[CuH_2L]^{2+}$ exists as the major species at pH 7 in equimolar solutions corresponds to $[CuH_{-2}LH_4]^{2+}$. Moreover, the deprotonation reactions at high pH values almost exclusively belong to the deprotonation of lysyl ammonium groups (e.g., $[CuHL]^{3+}$ to $[CuH_{-3}L]^{-}$) and these reactions are not accompanied by any spectral changes, with the exceptions of the peptides that contain His85 from the octarepeat domain of the protein. In this case, the deprotonations of four amide functions were suggested at high pH (species $[CuH_{-4}L]^{2-}$).[38] All these reactions, namely lysyl ammonium and especially the fourth amide deprotonations, take place under strongly alkaline conditions and their biological significance is probably negligible.

The most surprising observation from the speciation curves is related to the concentration of dinuclear complexes in equimolar solutions. Before the interpretation of these data, it has to be emphasised that the same trends were obtained for the mutants with two histidines, and the dinuclear complexes are always present in an amount of 20 to 50% in equimolar solutions above pH 5.5–6. At first sight, this suggests that the metal binding is strongly cooperative as reported in the literature for the octarepeat domain.[25,39] A more realistic mathematical or statistical approach to the complex formation reactions rules out the existence of such cooperation within these peptides. Table 3

  

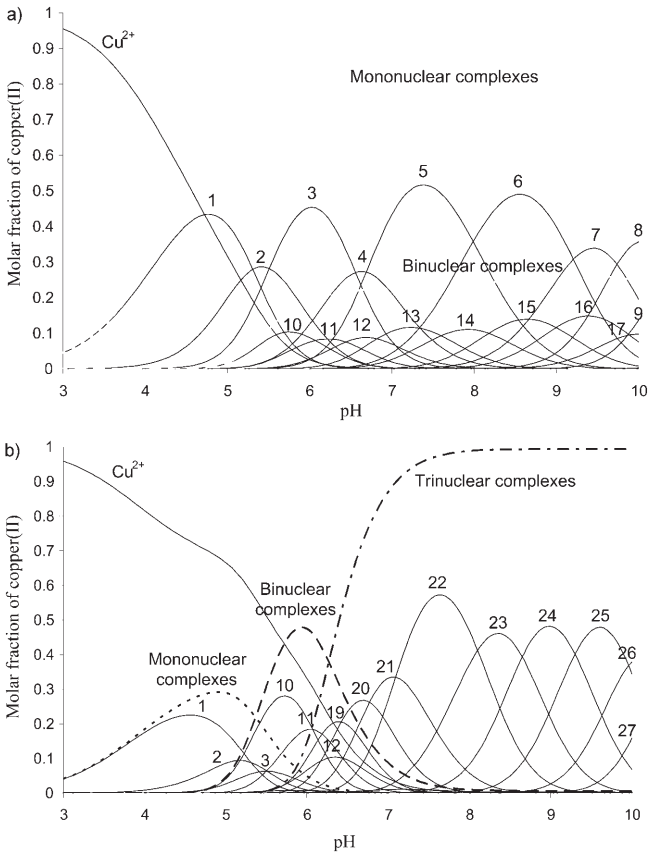


Figure 1. Species distribution of the complexes formed in the $Cu^{2+}$–HuPrP(84–114) system at a) 1:1 and b) 2.9:1 $Cu^{2+}$-to-ligand ratios. The complexes that were formed in less than 5% yield are omitted for clarity. $c_{HuPrP(84-114)} = 1.0$ mM; 1: $[CuH_6L]^{8+}$, 2: $[CuH_5L]^{7+}$, 3: $[CuH_4L]^{6+}$, 4: $[CuH_3L]^{5+}$, 5: $[CuH_2L]^{4+}$, 6: $[CuHL]^{3+}$, 7: $[CuL]^{2+}$, 8: $[CuH_{-1}L]^{+}$, 9: $[CuH_{-2}L]$, 10: $[Cu_2H_3L]^{7+}$, 11: $[Cu_2H_2L]^{6+}$, 12: $[Cu_2HL]^{5+}$, 13: $[Cu_2L]^{4+}$, 14: $[Cu_2H_{-1}L]^{3+}$, 15: $[Cu_2H_{-2}L]^{2+}$, 16: $[Cu_2H_{-3}L]^{+}$, 17: $[Cu_2H_{-4}L]$, 18: $[Cu_2H_{-5}L]^{-}$, 19: $[Cu_3L]^{6+}$, 20: $[Cu_3H_{-1}L]^{5+}$, 21: $[Cu_3H_{-2}L]^{4+}$, 22: $[Cu_3H_{-3}L]^{3+}$, 23: $[Cu_3H_{-4}L]^{2+}$, 24: $[Cu_3H_{-5}L]^{+}$, 25: $[Cu_3H_{-6}L]$, 26: $[Cu_3H_{-7}L]^{-}$, 27: $[Cu_3H_{-8}L]^{2-}$.

gives the percentage for the statistical distribution of the metal ions and ligands in a system when the complex formation is complete, and the metal ion and ligand are present in the same overall concentrations, but the ligand has three equivalent metal-binding sites. It is clear from Table 3 that dinuclear complexes statistically are expected in a concentration around 40%. This high concentration of the dinuclear species implies that there is no cooperation synergy in the complex-formation processes; on the contrary, it corresponds to the statistical distribution of the metal ions among the individual binding sites. Of course, the data in Table 3 are valid only if all of the binding sites are equivalent. In the case of prion fragments, this is not true, because in previous studies[29,34] we already demonstrated the increased metal-binding affinity of peptide fragments that contain His96 or His111 over that of the octarepeat monomers (e.g., His85). However, by using the stability constants reported for these fragments, the statistical distribution weighted by the different thermodynamic stabilities of the different binding sites can be calculated, and it is plotted in Figure 2. The comparison of the total concentrations of mono-, di-, and trinuclear complexes in Figures 1a and 2 makes it possible to evaluate the equivalency of binding sites, and also the existence of cooperation or antagonism in the metal binding. It is evident from these plots that the major tendency for the distribution of $Cu^{2+}$ among the various mono- and polynuclear species is similar both for the measured (Figure 1a), and for the statistically expected speciation (Figure 2a). On

Table 3. Statistical distribution of the ligand and metal ion among various species in which the ligand has three independent metal binding sites and the complex formation is complete.

| Stoichiometry | Ligand [%] | Metal ion [%] |
|---|---|---|
| 1:1 (M/L) samples | | |
| mononuclear | 44.4 | 44.4 |
| dinuclear | 22.2 | 44.4 |
| trinuclear | 3.7 | 11.1 |
| free ligand | 29.6 | – |
| 2:1 (M/L) samples | | |
| mononuclear | 22.2 | 11.1 |
| dinuclear | 44.4 | 44.4 |
| trinuclear | 29.6 | 44.4 |
| free ligand | 3.7 | |

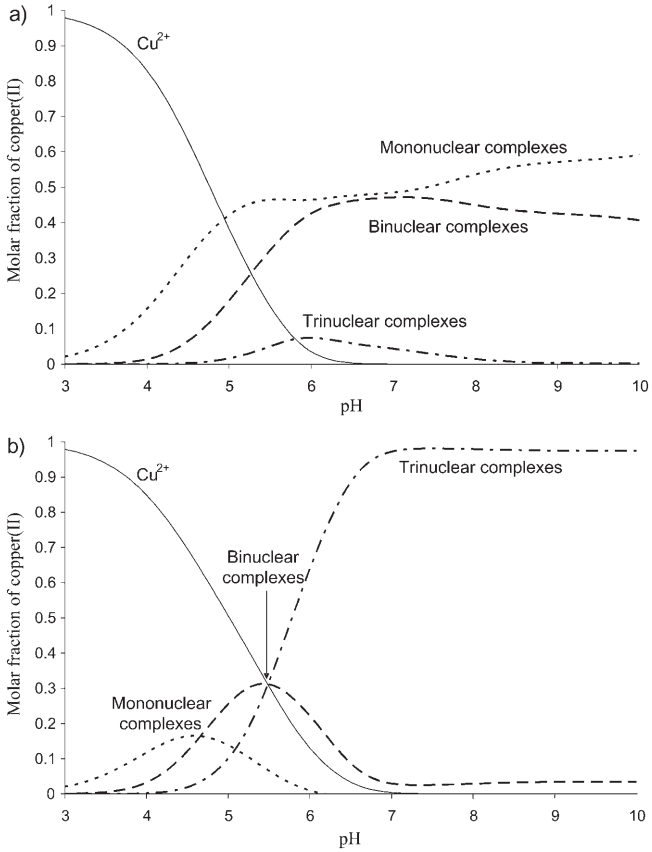


Figure 2. Expected distribution of mono- and polynuclear complexes of HuPrP(84–114) based on the stability constants of the 1-His peptide fragments at a) 1:1 and b) 2.9:1 $Cu^{2+}$-to-ligand ratios. No cooperative bonding was assumed.

  

the other hand, it is also evident from these figures that the total amounts of mono- and dinuclear species are different in the two cases. However, it should be taken into account that the values plotted in Figure 2 were obtained from a statistical distribution which was weighted by the stability constants of small peptide fragments that contain only one histidyl residue in each case. In the 31-mer peptide HuPrP-(84–114), the three histidines are present in the same molecule and they should influence the metal-binding affinity of each histidyl site; this results in some deviation from the statistical distribution. Moreover, some differences in the stability of the specific conformations required for the metal-ion coordination can be expected when comparing the small fragments with the 31-mer peptide. The total concentration of dinuclear species in Figure 1a is lower than that of Figure 2a, and this observation definitely rules out the possibility of the existence of any cooperation between one octarepeat monomer (His85) and the histidines outside the octarepeat domain (His96 and His111). From these speciation curves we can conclude that all the histidines are independent metal-binding sites, and their metal-binding affinities are more or less the same as those of the short peptide fragments. On the other hand, from these data we cannot deduce the metal-ion saturation of the various binding sites in the mono- and dinuclear species. Three coordination isomers of both mono- and dinuclear complexes can exist, but we cannot estimate their preferences from the equilibrium data. The spectroscopic data, especially CD spectroscopy, will give a reliable estimation for the ratio of these coordination isomers. It is also important to note that similar data were obtained for the peptides that contain two histidyl residues, but the speciation is simpler because trinuclear species are not formed. The dinuclear species are always present in equimolar samples and the percentage of them at pH 7 are 40, 39, 33 and 30% for HuPrP(84–114)His96Ala, HuPrP-(91–115), HuPrP(84–114)His85Ala, and HuPrP(84–114)His111Ala, respectively. These values are rather similar to each other and support the metal-binding ability of all sites in all peptides, although a small preference for binding at His111 can be estimated, and it will be further supported by the spectroscopic data.

**Binding modes of the ligands in various species**

*Species with binding of side-chain imidazole donor atoms ($N_{im}$), ($[CuH_6L]^{8+}$ to $[CuH_4L]^{6+}$)*: By taking into account the number of protonation sites of the ligands in the complexes with the highest protonation stages, namely in $[CuH_6L]^{8+}$ for HuPrP(84–114), and $[CuH_5L]^{7+}$ for the 2-histidine-containing mutants, we can conclude that $Cu^{2+}$ can only be coordinated through a single imidazole nitrogen donor atom; this assumption is supported by both equilibrium and spectroscopic data. The direct comparison of thermodynamic parameters in Table 2 might be misleading because of the different protonation states of the ligands; thus, some other equilibrium parameters have been calculated from the primary data and they are presented in Table 4. The data in the first three rows of Table 4 correspond to the stability constants of the species that are coordinated only through one, two or three imidazole donor atoms and all other metal-binding sites are protonated. The $\log K(Cu+N_{im})$ values for simple monodentate binding are around 4.0 log units, and they are similar to those reported for the short fragments, or other peptides with the coordination of a single histidyl residue.[29,34,35] On the other hand, the $\log K(Cu+2N_{im})$ values strongly support the involvement of both non-protonated histidyl residues in the metal binding in the species $[CuH_5L]^{7+}$ of HuPrP(84–114) and $[CuH_4L]^{6+}$ of the 2-histidine mutants, which is possible in the form of macrochelate or loop structures. In the case of the 3-histidine peptide, the formation of three different macrochelates (His85+His96, His85+His111, or His96+His111) is possible, and it results in the existence of coordination isomers. No spectroscopic technique is available to distinguish between these isomers, but the stability constants of the two 2-histidine peptides in Table 4 can help to estimate the preference of isomers. The $\log K(Cu+2N_{im})$ data reveal that the macrochelation is favoured for HuPrP(84–114)His111Ala. It strongly suggests that the macrochelate that is formed with the involvement of His85 and His96 is preferred over the others (see Scheme 1a). This finding is to be expected because the peptide chain is flexible between His85 and His96, but there are two prolyl residues (102 and 105) between His96 and His111, which can create some

Table 4. Calculated equilibrium parameters for the $Cu^{2+}$ complexes of peptide fragments of prion protein ($T=298$ K, $I=0.2$ mol dm$^{-3}$ KCl).

| Process | HuPrP(84–114) | HuPrP(91–115) | HuPrP(84–114)His85Ala | HuPrP(84–114)His96Ala | HuPrP(84–114)His111Ala |
|---|---|---|---|---|---|
| $\log K(Cu+N_{im})$ | 4.33 | 4.02 | 3.54 | 3.71 | 4.43 |
| $\log K(Cu+2N_{im})$ | 5.21 | 4.83 | 4.55 | 4.71 | 5.60 |
| $\log K(Cu+3N_{im})$ | 6.47 | – | – | – | – |
| $pK_1$(monomer) | 6.56 | 5.92 | 5.93 | 5.89 | 6.25 |
| $pK_2$(monomer) | 6.69 | 6.29 | 6.13 | 6.70 | 6.98 |
| $pK_{12av}$(monomer) | 6.63 | 6.11 | 6.03 | 6.30 | 6.62 |
| $pK_3$(monomer) | 7.99 | 7.76 | 7.54 | 7.97 | 8.47 |
| $pK_{3(1)}$(dimer) | 7.60 | 7.29 | 7.29 | 7.53 | 7.86 |
| $pK_{3(2)}$(dimer) | 8.18 | 8.12 | 7.89 | 8.74 | 9.13 |
| $pK_{3(1)}$(trimer) | 7.09 | – | – | – | – |
| $pK_{3(2)}$(trimer) | 8.10 | – | – | – | – |
| $pK_{3(3)}$(trimer) | 9.00 | – | – | – | – |

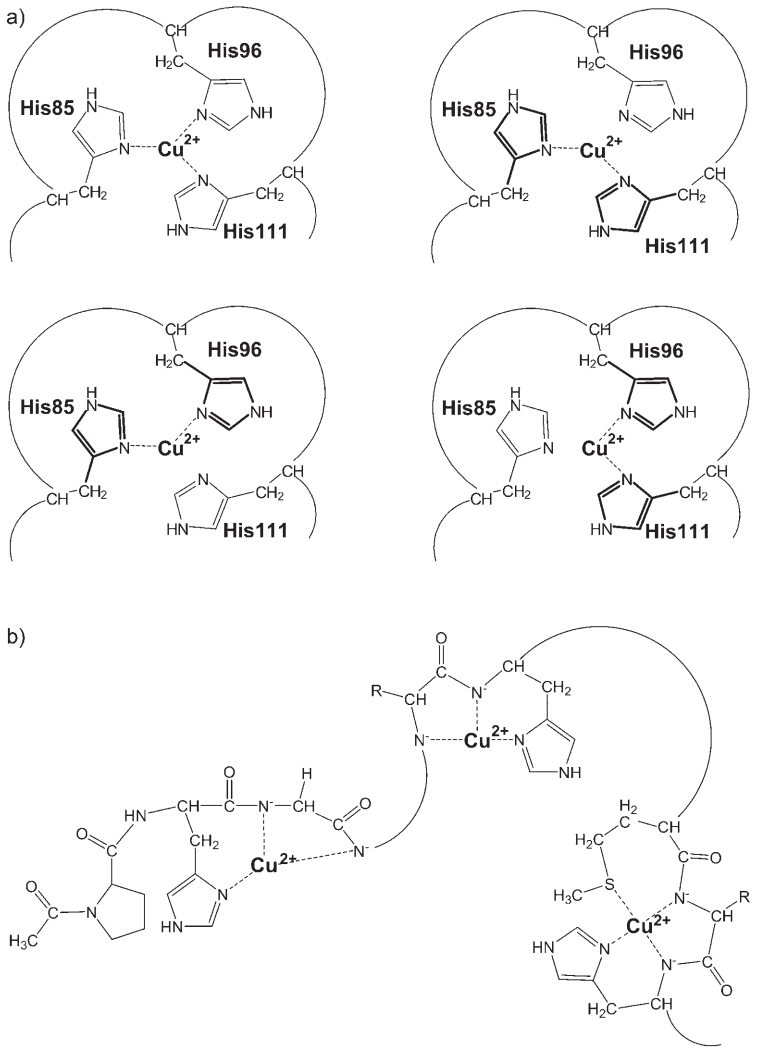


Scheme 1. a) Schematic representation of the possible macrochelate complexes in $Cu^{2+}$–HuPrP(84-114) and b) major species present at physiological pH, when all histidines are independent binding sites.

steric hindrance for the chain folding.[40] The data reported for the $3N_{im}$-macrochelate of HuPrP(84–114) provide further support for macrochelation. The value of $\log K(Cu+3N_{im}) = 6.47$ was obtained for the $[CuH_4L]^{6+}$ species of the 31-mer peptide, while 7.22 and 8.08 were published for the small 3-histidine peptides Ac-HisHisGlyHis-NHMe and Ac-HisAlaHisValHis-$NH_2$, respectively; these peptides have similar binding modes.[41,42] According to these data, the stabilities of the macrochelates follow the order HAHVH > HHGH > HuPrP(84–114). The formation of macrochelates with the exclusive metal binding of side-chain imidazole functions have been reported for a series of other peptides that contain two or three histidyl residues and the stability constants were also in the same range.[43–50] These observations suggest that macrochelation can occur with any multihistidine peptides, but the stability is a measure of the distance between the histidyl residues. In the case of HHGH, the imidazoles are too close to each other, while for HuPrP(84–114) and it mutants they are too far apart, but the involvement of His85 and His96 is the most-preferred variant among the three possible isomers.

UV/Vis, CD, and EPR spectra of all $Cu^{2+}$–peptide systems have been recorded at three [for HuPrP(84–114)] or two (for the mutants) metal-to-ligand ratios and at many different pH values in the range from $3.5 < pH < 11.0$. Two sets of the visible absorption spectra of the $Cu^{2+}$–HuPrP(84–114)His111Ala system are shown in Figure 3; they reflect the high similarity of the data and the continuous shift of absorption maxima with increasing pH at the two different ratios. The PSEQUAD computer program[51] generally makes it possible to calculate the individual spectra of the major species in solution, but this type of calculation is not possible for these peptide complexes because too many species are present (see Figure 1). Figure 1 reveals the overlap of at least 4–5 species at all pH values; this rules out the reliable differentiation of the small changes of the spectral parameters that are related to the different $Cu^{2+}$ complexes. The continuous blue shift, however, corresponds very well to the increase in the number of coordinated nitrogen donors. It is also evident from the data that both the blue shift and the intensity of absorption spectra become more significant above pH 5.5–6, which is when the amide-coordinated species start to form. In the pH range from 4–5.5, only low-intensity absorption spectra can be recorded at the wavelength maxima around 700–750 nm, which is in agreement with the hypothesis that the imidazole nitrogen atoms bind exclusively.

CD spectra of the $Cu^{2+}$–HuPrP(84–114) system that were obtained at three different metal-to-ligand ratios are plotted in Figure 4. It is clear from Figure 4 that the CD parameters are more sensitive to the metal-to-ligand ratio than those of the UV/Vis and EPR spectra, and the extrema can be used to rationalise the existence of coordination isomers. It is also important to observe that in the range of d–d transitions, measurable CD activity of the samples can be recorded only above pH 5.5–6. This implicates the involvement of peptide amide groups in the metal binding. The absorption maxima of the same samples provide an indirect proof for the exclusive metal-ion coordination of the side-chain imid-

  

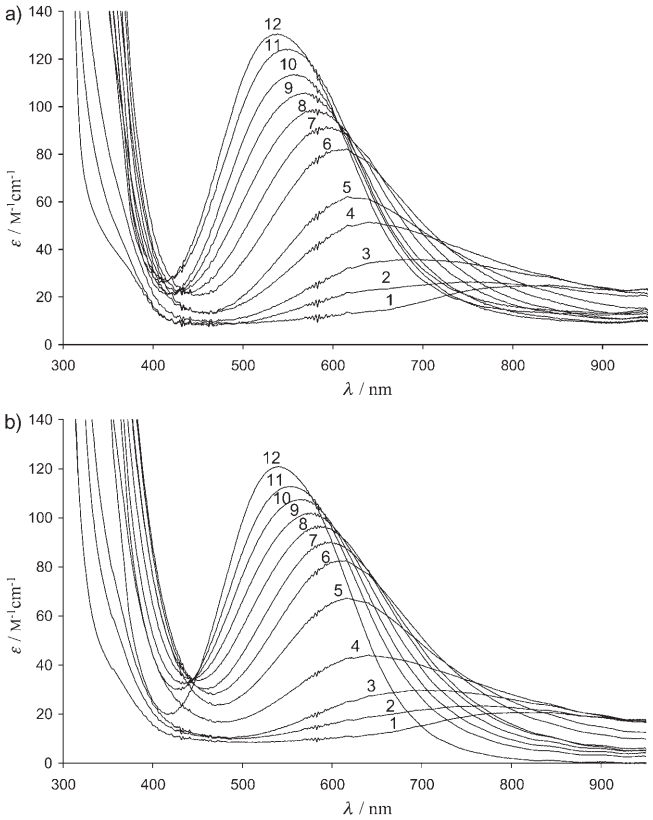


Figure 3. Molar UV/Vis spectra of the $Cu^{2+}$–HuPrP(84–114)His111Ala system at a) 1:1 and b) 2:1 $Cu^{2+}$-to-ligand ratios as a function of pH. $c_{HuPrP(84–114)His111Ala}$ = 0.77 mM in both cases. At a 1:1 M/L ratio, pH 3.59 (1), 5.06 (2), 5.59 (3), 6.12 (4), 6.46 (5), 6.93 (6), 7.39 (7), 7.83 (8), 8.32 (9), 8.82 (10), 9.24 (11), 9.87–11.18 (12); at 2:1 ratio, pH 3.66(1), 4.89 (2), 5.51 (3), 6.16 (4), 6.59 (5), 6.99 (6), 7.47 (7), 7.90 (8), 8.35 (9), 8.85 (10), 9.36 (11), 9.91–11.20 (12).

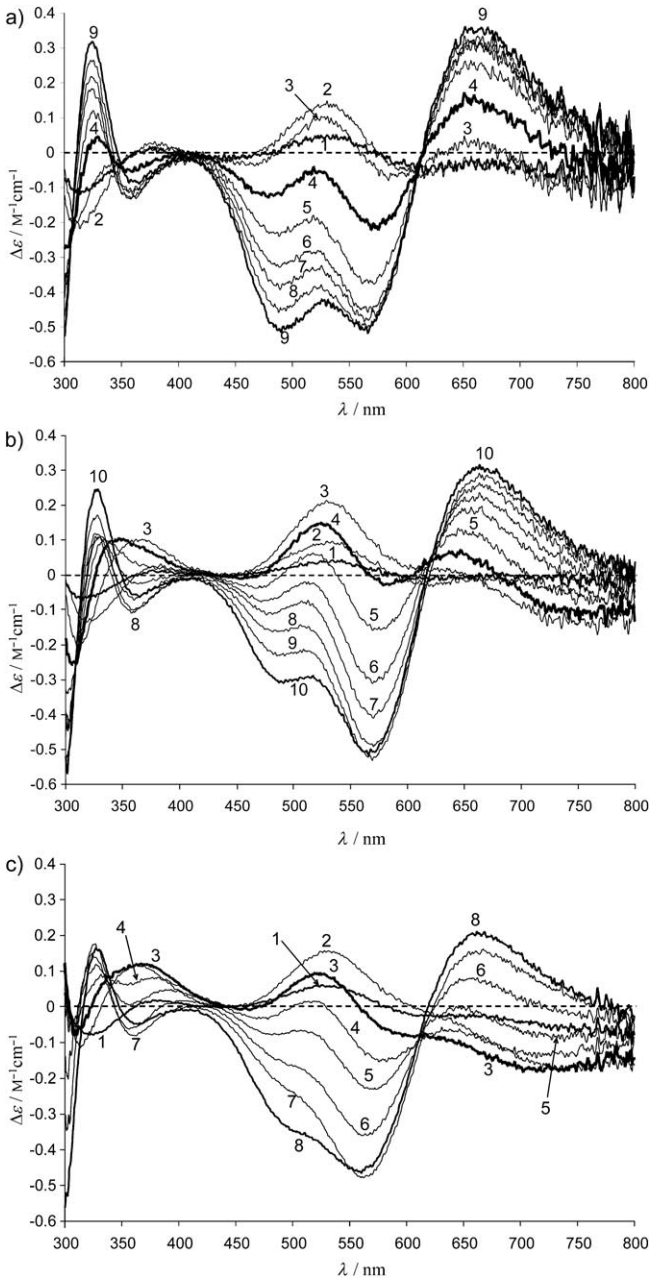


Figure 4. Molar CD spectra of the $Cu^{2+}$–HuPrP(84–114) system at a) 1:1, b) 2:1 and c) 3:1 $Cu^{2+}$-to-ligand ratios as a function of pH. $c_{HuPrP(84–114)}$ = 0.65 mM in all cases. At 1:1 ratio, pH 6.05 (1), 6.84 (2), 7.33 (3), 7.99 (4), 8.71 (5), 9.56 (6), 10.00 (7), 10.63 (8), 11.32 (9); at a 2:1 ratio, pH 5.81 (1), 6.06 (2), 6.93 (3), 7.50 (4), 7.98 (5), 8.48 (6), 8.95 (7), 9.64 (8), 10.44 (9), 11.25 (10); at a 3:1 ratio, pH 6.00 (1), 6.78 (2), 7.42 (3), 7.91 (4), 8.43 (5), 9.25 (6), 10.16 (7), 11.33 (8).

azole residues, which are rather far from the chirality centres of the molecules.

Low-temperature EPR spectroscopy is generally the most sensitive technique to distinguish between different coordination geometries and binding modes of $Cu^{2+}$ complexes. The EPR spectra of the $Cu^{2+}$–HuPrP(84–114) system that were recorded at 1:1 and 3:1 M/L ratios are shown in Figure 5, and these spectra seem to contradict this expectation. The pH-dependent EPR spectra of these systems are rather simple and reflect the presence of only a few different $Cu^{2+}$ species. However, it should be taken into account that EPR spectroscopy can differentiate only between the species with different numbers of coordinated nitrogen donors, and as a consequence, the coordination isomers formed with the three independent histidyl residues have more or less the same effects on the EPR parameters. The three binding sites (His85, 96, and 111) of the 31-mer peptide are far enough from each other, and the paramagnetic probes (i.e., the $Cu^{2+}$ ions) do not show any magnetic interaction. The unfavourable consequence is that, because the three binding sites are very similar to each other, the measured EPR spectra resemble those that would be obtained in the case of a system that is formed by a $Cu^{2+}$ ion interacting with three ligands that are very similar to each other. In our previous publications[41,42] the parameters $A_{\parallel} \approx 160$–170 and 170–180 ($\times 10^{-4}$ cm$^{-1}$) and $g_{\parallel} = 2.30$–2.31 and 2.26–2.28 were reported for the macrochelates that were formed by the coordination of $2N_{im}$- and $3N_{im}$-donor atoms. The EPR spectra measured in the $Cu^{2+}$–HuPrP systems show the coexistence of at least two or three species in slightly acidic solution. In equimolar solutions and at pH values of 4.95 and

  

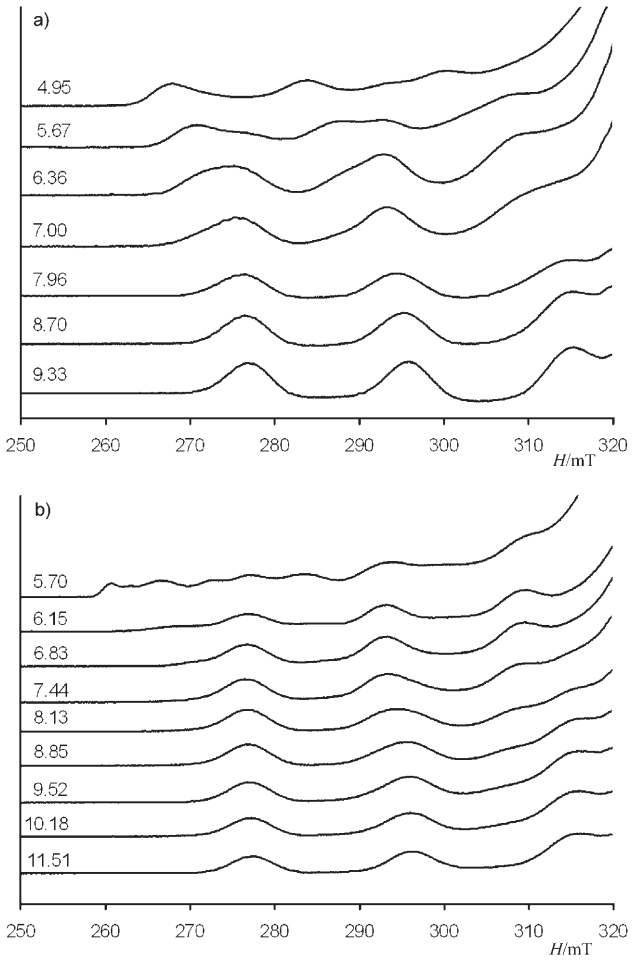


Figure 5. EPR spectra of the $Cu^{2+}$–HuPrP(84–114) system at a) 1:1 and b) 3:1 $Cu^{2+}$-to-ligand ratios as a function of pH. $C_{Cu^{2+}} = 1.0$ mM in both cases. pH Values are written on the spectra.

5.67 the parameters $A_{\parallel} = 172$ and 182 ($\times 10^{-4}$ cm$^{-1}$) and $g_{\parallel} =$ 2.288 and 2.261, respectively, can be calculated, and they suggest the predominance of the $2N_{im}$ and $3N_{im}$ species at these pH values. According to the speciation curves, these complexes should predominate at slightly higher pH values, but the effect of different temperatures should also be considered. The complexes with more nitrogen donors are generally formed in more exothermic reactions, thus lowering the temperature will shift the equilibria towards the formation of 2N- and 3N-complexes; this supports the detection of these species in slightly more acidic solution.

*Species with ($N_{im}$,$N^-$)-, and ($N_{im}$,$N^-$,$N^-$)-coordination modes ($[CuH_3L]^{5+}$ and $[CuH_2L]^{4+}$)*: Both UV/Vis and EPR spectroscopic techniques unambiguously prove the formation of amide-bonded species above pH 5.5–6.0. Similar observations were reported for the short peptide fragments of prion proteins, and in most cases the deprotonation of two amide functions took place cooperatively. This results in the formation of 3N-complexes as the major species in the physiological pH range.[29] The results obtained for the multi-histidine fragments studied in this work, however, indicate the existence of the intermediate 2N-complexes in measurable concentration. The p$K$ values of successive amide deprotonation are listed in Table 4, and the comparison of the data suggests that the existence of macrochelates is responsible for both the presence of 2N-complexes, and the shift of amide deprotonation to slightly higher pH ranges. In the case of the corresponding short fragments, only the averages of the first two deprotonations were calculated, and the values ranged between 5.64 and 6.08. In the case of HuPrP(84–114) and the mutants, the p$K_{12av}$(monomer) values are in the range from 6.03 to 6.63; this reflects a slightly less-favoured amide deprotonation. The stepwise p$K$ values reveal the same tendencies, and it is also notable that the highest p$K$ values belong to HuPrP(84–114) and HuPrP(84–114)His111Ala in all cases. The high values obtained for the latter ligand support the preference of macrochelation with the involvement of the His85 and His96 residues. On one hand the ($N_{im}$,$N_{im}$)-macrochelates slightly shift the deprotonation and amide binding to higher pH values, on the other hand, the coordination of a second imidazole donor atom in the form of a macrochelate enhances the thermodynamic stability of the ($N_{im}$,$N^-$)-chelate, which results in the loss of cooperation. The small difference between p$K_1$(monomer) and p$K_2$(monomer) values, however, suggests that the [($N_{im}$,$N^-$)+$N_{im}$]-coordinated complexes are only minor species, and that spectroscopic parameters cannot be determined for $[CuH_3L]^{5+}$. Nevertheless, the EPR spectra of equimolar solutions of $Cu^{2+}$ and HuPrP(84–114) at pH $\approx$6.4 showed the signals of a species with parameters intermediate between those of the complexes with ($N_{im}$,$N^-$)- and ($N_{im}$,$N^-$,$N^-$)-coordination. These signals can be reasonably assigned to the species $[CuH_3L]^{5+}$, which has the [($N_{im}$,$N^-$)+$N_{im}$]-coordination mode. The continuous blue shift of the visible spectra with increasing pH provides further support for this assumption because the absorption maxima of the above-mentioned coordination mode should be between those of macrochelates ($\approx$700 nm) and ($N_{im}$,$N^-$,$N^-$)-complexes ($\approx$600 nm).

Both potentiometric and spectroscopic data prove that the ($N_{im}$,$N^-$,$N^-$)-chelated species predominate around pH 7 in all systems. The stoichiometry of this species is $[CuH_2L]^{4+}$, and because of its high concentration, its spectral parameters can be estimated with relatively high accuracy. These values are included in Table 5 together with those of the 4N-complexes that dominate in alkaline solutions. The range of spectroscopic parameters listed in Table 5 is in reasonable agreement with those reported for the short fragments with single histidyl residues. There are at least three major reasons why the complete agreement of these data is not possible: i) the binding modes of the species are similar, but the charge of the species and the conformation of the short and 31-mer peptides are different; ii) the basic coordination mode is ($N_{im}$,$N^-$,$N^-$), but it is supported by the metal binding of the other histidyl residues in the form of macrochelates; this results in an increase of the total number of coordinated nitrogen donors; and iii) different coordination

  

Table 5. Estimated spectroscopic parameters of the major $Cu^{2+}$ species formed with the peptide fragments of prion protein.

| Process | HuPrP(84–114) | HuPrP(91–115) | HuPrP(84–114)His85Ala | HuPrP(84–114)His96Ala | HuPrP(84–114)His111Ala |
|---|---|---|---|---|---|
| $[(N_{im},N^-,N^-)+N_{im}]$ coordination mode ($[CuH_2L]^{4+}$) | | | | | |
| UV/Vis $\lambda_{max}$ [nm]/$\varepsilon$ [$M^{-1}cm^{-1}$] | 600/105 | 608/112 | 609/95 | 610/113 | 600/92 |
| EPR spectra $g_{\parallel}/A_{\parallel}$ [$\times10^{-4}$ $cm^{-1}$] | 2.223/175 | 2.217/190 | | 2.230/167 | 2.221/186 |
| CD spectra $\lambda$ [nm]/$\Delta\varepsilon$ [$M^{-1}cm^{-1}$] | 308/−0.22 | 312/−0.36 | 315/−0.35 | 334/−0.16 | 340/+0.37 |
| | 465/−0.03 | 374/+0.09 | 372/+0.11 | 384/+0.04 | 498/+0.18 |
| | 529/+0.11 | 524/+0.29 | 523/+0.33 | 478/−0.13 | 590/−0.15 |
| | 586/−0.06 | 605/−0.17 | 608/−0.12 | 576/+0.24[a] | 705/−0.16 |
| | 657/+0.03 | 790/−0.15 | 800/−0.15 | | |
| | 780/−0.08 | | | 760/−0.13 | |
| $[N_{im},N^-,N^-,N^-]$ coordination mode ($[CuHL]^{3+}$–$[CuH_{-3}L]^-$) | | | | | |
| UV/Vis $\lambda_{max}$ [nm]/$\varepsilon$ [$M^{-1}cm^{-1}$] | 525/135 | 535/135 | 536/125 | 533/133 | 535/128 |
| EPR spectra $g_{\parallel}/A_{\parallel}$ [$\times10^{-4}$ $cm^{-1}$] | 2.196/195 | 2.200/199 | 2.199/200 | 2.192/198 | 2.195/203 |
| CD spectra $\lambda$ [nm]/$\Delta\varepsilon$ [$M^{-1}cm^{-1}$] | 321/+0.14 | 323/+0.19 | 325/+0.10 | 315/+1.10 | 305/−1.27 |
| | 355/−0.11 | 355/−0.11 | 355/−0.11 | 358/−0.12 | 494/+0.67 |
| | 484/−0.28 | 481/−0.20 | 475/−0.08 | 495/−1.11 | 589/−1.10 |
| | 566/−0.42 | 566/−0.38 | 572/−0.43 | 628/+0.85 | |
| | 655/+0.29 | 655/+0.29 | 660/+0.24 | | |

[a] Broad band.

isomers of $[CuH_2L]^{4+}$ exist because all of the histidines can be metal-binding sites. For example, when only two histidines are present in the peptides as is the case in HuPrP(91–115), either His96 or His111 can be the primary chelating site, while the other histidine forms the macrochelate, which is a weak interaction and can exist either in a closed or open form. Altogether, it means that four coordination isomers ($2\times2$) for the 2-histidine peptides, and nine isomers ($3\times3$) for HuPrP(84–114) are possible. Of course, the probability for the formation of these isomers is not the same, but UV/Vis and EPR spectroscopic techniques cannot be used to differentiate among them. The CD spectra of the isomers bonded to different histidyl residues are, however, different and these data can be used to estimate the preference for isomers, as will be described later.

*Species with the ($N_{im}$,$N^-$,$N^-$,$N^-$)-coordination mode ($[CuHL]^{3+}$ to $[CuH_{-3}L]^-$)*: Very characteristic spectral changes can be observed in all systems in the pH range from 6.5 to 9 at any metal-to-ligand ratio. The significant blue shift of the absorption spectra and the decrease of $g_{\parallel}/A_{\parallel}$ values correspond very well to the increase of nitrogen donors, that is, the formation 4N-coordinated complexes. It is also important to note that a further increase in pH does not result in measurable spectral changes because only the deprotonation of lysyl ammonium groups occur above pH 9. As a consequence, there is a wide range for the stoichiometries of 4N complexes, including the species from $[CuHL]^{3+}$ (i.e., $[CuH_{-3}LH_4]^{3+}$) to $[CuH_{-3}L]^-$. The p$K$ values for the deprotonation of the third amide functions are listed in Table 4 and cover the range between 7.54 and 8.47. These values are slightly higher than those reported for the corresponding nonapeptides[29,34] and they provide further support for the macrochelation in the species $[CuH_2L]^{4+}$ as was discussed previously.

Important conclusions can be drawn from the comparison of the EPR parameters of the $[CuH_2L]^{4+}$ and $[CuHL]^{3+}$ complexes. Namely, the data for the latter species are more or less the same for all ligands, while the EPR parameters of the former species vary in a relatively wide range. This can be explained by the decrease in the number of coordination isomers. The equatorial coordination sites of $[CuHL]^{3+}$ are saturated; there is no chance for macrochelation, and only three isomers of HuPrP(84–114) (only two for the mutants) can form that differ only in the location of the histidyl residues that are involved in metal binding (His85, His96 or His111). CD spectra of both $[CuH_2L]^{4+}$ and $[CuHL]^{3+}$ species are, however, significantly different, because this technique is sensitive to the number and to the type of coordinated donor functions, and to the amino acids involved in the Cu–$N^-$ bond. In the case of His85, the 4N-chelate includes the HGGG sequence towards the C termini, while in the case of His96 and His111, the GTH and MKH sequences, respectively, are included at the N-terminal side of both His residues. The significantly different CD parameters of these short peptide fragments have already been reported in our previous publications, and now they are presented in Figure 6,[29,34] while Figure 7 shows the CD spectra of $[CuH_2L]^{4+}$ and $[CuHL]^{3+}$ species of HuPrP(84–114) and its 2-histidine-containing mutants. The similarities and differences in the CD spectra are striking and make it possible to estimate the ratios of various coordination isomers. Similarities of the spectra for HuPrP(91–115) (2) and HuPrP(84–114)His85Ala (3) indicate that the length of the peptide has only a weak effect on the molar spectra. At the same time, the comparison of the spectra for HuPrP(84–114) (1, bold line) and the two His mutants suggests at first glance that the coordination sites of HuPrP(84–114) are the most similar to that of HuPrP(91–115) and HuPrP(84–114)His85Ala, especially at high pH, that is, in the $[CuHL]^{3+}$ species His96 and His111 are the main copper-binding sites. At lower pH, however, based on the smaller similarity between HuPrP(84–114) and HuPrP(91–115), or HuPrP(84–114)His85Ala, it can be said that His85 also has a measurable contribution to the $Cu^{2+}$ coordination, as expected from the comparison of the stability-constant values for the 1-His species.[34]

  

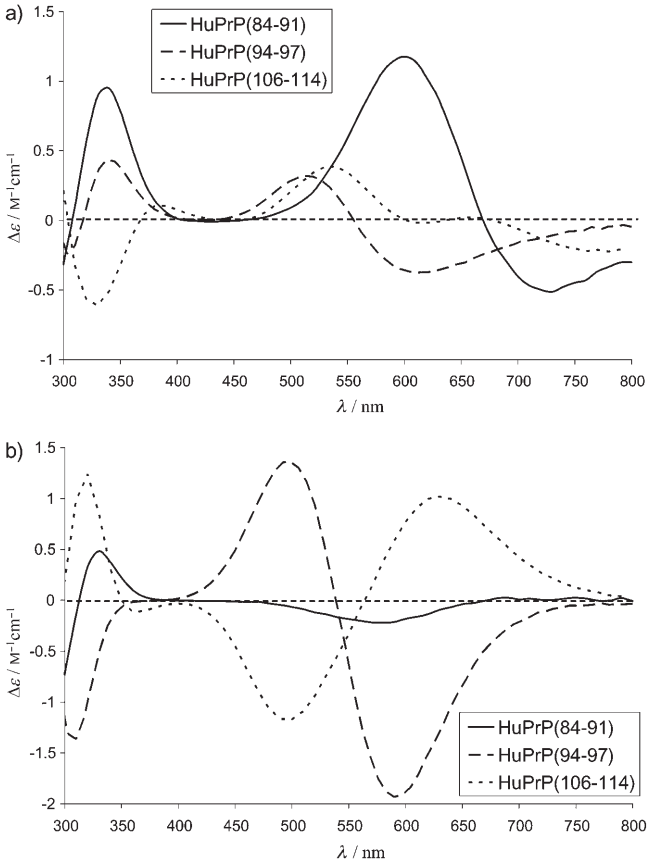


Figure 6. Molar CD spectra of the individual $Cu^{2+}$-binding sites of HuPrP(84–114) for the a) [$N_{im}$, $2\times N^-$] and b) [$N_{im}$, $3\times N^-$] coordinated complexes, calculated by PSEQUAD.

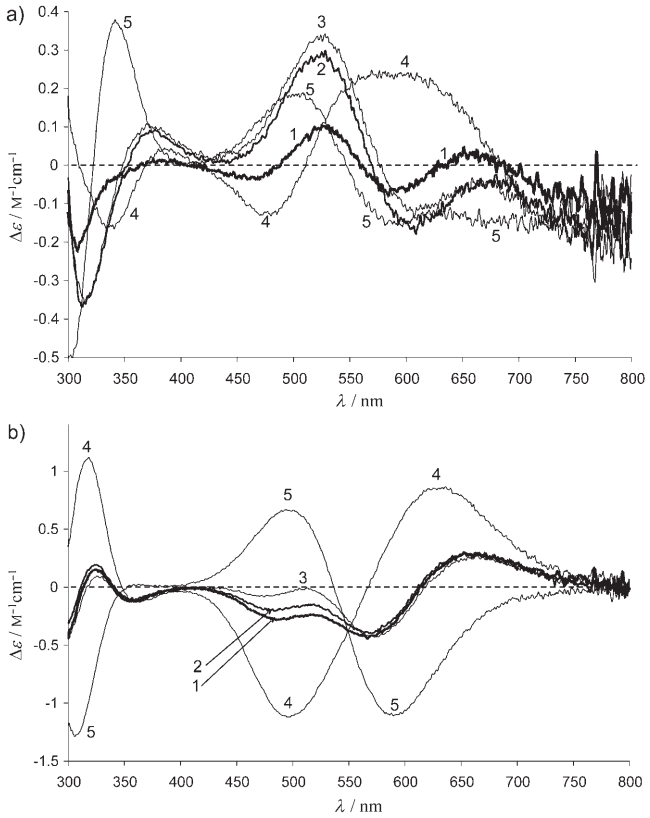


Figure 7. Measured molar CD spectra in the $Cu^{2+}$–HuPrP(84–114) (1), $Cu^{2+}$–HuPrP(91–115) (2), $Cu^{2+}$–HuPrP(84–114)His85Ala (3), $Cu^{2+}$–HuPrP(84–114)His96Ala (4) and $Cu^{2+}$–HuPrP(84–114)His111Ala (5) systems for the a) [$N_{im}$, $2\times N^-$] and b) [$N_{im}$, $3\times N^-$] coordination modes.

However, it should be taken into account that well-measured CD extrema are obtained only for the amide-bonded species of peptides, so we did not calculate the existence of coordination isomers of species below pH 6, for example, for the simple macrochelates. By using the CD spectra of all individual short fragments (Ac-PHGGGWGQ-$NH_2$, Ac-GTHS-$NH_2$, and Ac-KTNMKHMAG-$NH_2$ including His85, His96, and His111, respectively) and the pH-dependent EPR spectra of HuPrP(84–114) (see Figure 5), we can estimate the preference of metal-binding sites and the results of these calculations are shown by Figure 8 in the pH range from 6–11. It is clear from Figure 8 that metal binding via His111 and His96 is much preferred over His85, in agreement with the previous results that were reported for the small fragments.

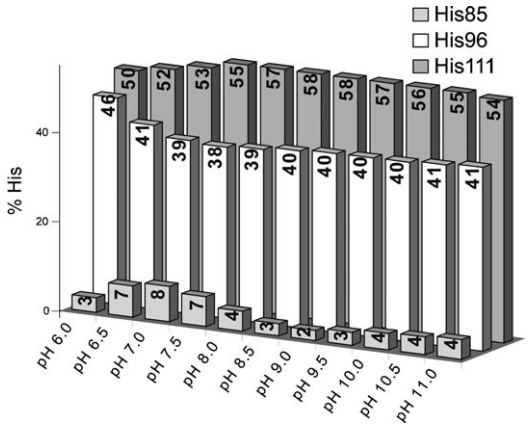


Figure 8. Distribution of $Cu^{2+}$ among the three histidines of HuPrP(84–114) at 1:1 $Cu^{2+}$ to ligand ratio as calculated from the measured CD spectra of the $Cu^{2+}$–HuPrP(84–114) 1:1 system. $c_{HuPrP(84-114)}$ = 0.65 mM.

**Formation of di- and trinuclear complexes**: It has already been discussed that the formation of dinuclear complexes of 2-histidine peptides and di- and trinuclear complexes of HuPrP(84–114), even in equimolar solutions, suggests the independence of the metal-binding sites of these peptides (see Figure 2), but the application of ESI-MS provided the most unambiguous proof for the formation of these species. Before the interpretation of the mass spectrometric results, it is important to note the complexity of these spectra. An enormous number of peaks appeared in the mass spectra of all systems, and it is not surprising if one takes into account the speciation curves (see Figure 1) and the different charges of the various species. Careful analysis of the spectra, however, always indicated the existence of dinuclear species

  

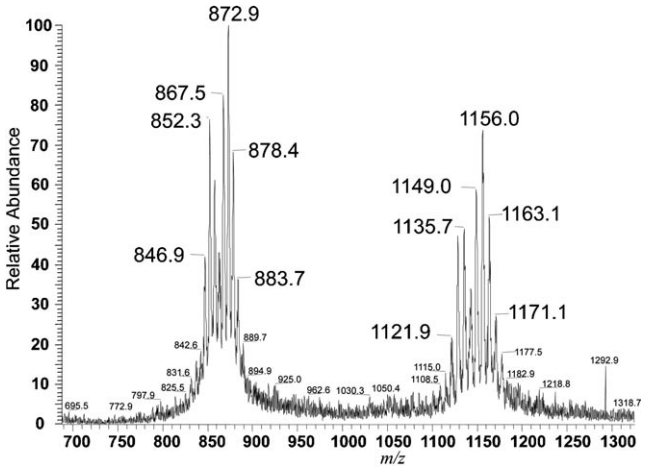


Figure 9. ESI-MS spectrum of the $Cu^{2+}$–HuPrP(84–114) system at 1:1 $Cu^{2+}$ to ligand ratio and pH 10.0. $c_{HuPrP(84-114)} = c_{copper(II)} = 1 \times 10^{-5}$ M. The identified peaks are as follows: $m/z$: 846.9 $[CuHLNa]^{4+}$, 852.3 $[H_{-1}LNa_5]^{4+}$, 867.5 $[Cu_2H_{-2}LNa_2]^{4+}$, 872.9 $[Cu_2H_{-3}LNa_3]^{4+}$, 878.4 $[Cu_2H_{-4}LNa_4]^{4+}$, 883.7 $[Cu_2H_{-5}LNa_5]^{4+}$, 1121.9 $[LNa_3]^{3+}$, 1135.7 $[CuH_{-1}LNa_2]^{3+}$, 1149.0 $[Cu_2H_{-2}LNa]^{3+}$, 1156.0 $[Cu_2H_{-3}LNa_2]^{3+}$, 1163 $[Cu_2H_{-4}LNa_3]^{3+}$, 1171.1 $[Cu_2H_{-5}LNa_4]^{3+}$.

in equimolar solutions, and even the presence of the two major isotopes of copper was reflected in the mass spectra. A part of the ESI-MS spectra of $Cu^{2+}$–HuPrP(84–114) system that was obtained in equimolar solution is presented in Figure 9. It is clear from Figure 9 that peaks of both the free ligand and the mono- and dinuclear complexes can be assigned in equimolar samples at high pH values when all histidyl residues are independent metal-binding sites.

On the other hand, both the stoichiometries of polynuclear species and the speciation curves reveal that the formation of di- and trinuclear complexes is connected to the involvement of the amide nitrogen atoms in metal binding. Monodentate binding of independent histidines through the $N_{im}$-donor atoms should have the $[Cu_2H_4L]^{8+}$ (or more protonated) overall stoichiometry, but stability constants can be calculated only for $[Cu_2H_3L]^{7+}$ and the less-protonated counterparts. It can be easily explained by the preference for macrochelation when $N_{im}$ atoms are the exclusive metal-binding sites. Even the species $[Cu_2H_3L]^{7+}$ and $[Cu_2H_2L]^{6+}$ are present in rather low concentration, and the first major species among the dinuclear complexes is $[Cu_2L]^{4+}$. This species predominates around pH 7 and all spectral parameters are characteristic of those reported for the 3N-complexes in Table 5. As a consequence, this species corresponds to the stoichiometry $[Cu_2H_{-4}LH_4]$, which contains two metal ions in the $(N_{im},N^-,N^-)$-coordination environment and four protonated lysyl residues. Further, two deprotonation reactions take place around pH 8 and these are accompanied with the spectral changes characteristic of $(N_{im},N^-,N^-,N^-)$-coordination ($[Cu_2H_{-1}L]^{3+}$ and $[Cu_2H_{-2}L]^{2+}$). Deprotonation p$K$ values of these amide functions are also listed in Table 5 [p$K_{3(1)}$(dimer) and p$K_{3(2)}$(dimer)] and the values reflect that the binding of the third amide function at the first site is facilitated, while the second one is slightly suppressed compared to the mononuclear species. The enhanced stability of $[Cu_2H_{-1}L]^{3+}$ probably comes from the lack of macrochelate in dinuclear species.

Trinuclear complexes are formed only with HuPrP(84–114), which contains three independent histidyl residues. In this case, the major species around pH 7 is $[Cu_3H_{-2}L]^{4+}$ with $3\times(N_{im},N^-,N^-)$-coordination mode and it is transformed in three steps (see p$K_3$(trimer) in Table 5) to $[Cu_3H_{-5}L]^{+}$ of which, the spectral parameters are characteristic of $3\times(N_{im},N^-,N^-,N^-)$-coordination. The corresponding equilibrium data in Table 5 reflect the same tendencies as discussed for the dinuclear species, and can be explained by the lack of macrochelates and different charges of various species. The high similarity of the two or three metal-binding sites of these peptides do not make it possible to determine the individual spectroscopic parameters for each species, but it is evident from Figure 3 that the visible absorption maxima occur at the same wavelength, but with doubled intensity compared to the monomers. The agreement of the EPR spectra that were obtained at 1:1 and 3:1 metal-to-ligand ratios are even more evident and support the same coordination environment of $Cu^{2+}$. On the other hand, the CD extrema of the systems depend on the metal-to-ligand ratios, because their intensity is a function of the chiral distribution from the amino acids present in the vicinity of the particular histidyl residues.

## Conclusion

In the present study, the combined potentiometric and spectroscopic (UV/Vis, CD and EPR spectroscopy and ESI-MS) approach revealed the high $Cu^{2+}$-binding affinity of all peptide fragments as well the coordination mode of the peptides in the different complex species. The complex formation between $Cu^{2+}$ ion and the peptides starts in acidic solution, above pH 3, and becomes almost complete by the physiological pH range. Imidazole nitrogen donor atoms of histidyl residues are the exclusive metal-binding sites below pH 5.5 and they have a preference for the formation of macrochelate structures (see Scheme 1a). Our results indicate a preferential macrochelate formation that involves histidines 85 and 96 over the other two possibilities, which come by considering histidine 85 and 111 or 96 and 111. Of course, this result is derived from the $Cu^{2+}$–peptide model systems, and, at the present stage, cannot be extended to the whole protein. The deprotonation and metal-ion coordination of amide functions take place by increasing the pH, and all of the histidines can be considered to be independent metal-binding sites in these species. As a consequence, di- and trinuclear complexes can be formed even at equimolar metal ion/peptide concentration, but the ratio of polynuclear species does not exceed the statistically expected one. Thus, this rules out any cooperation in $Cu^{2+}$ binding. The species with the $(N_{im},N^-,N^-)$-binding mode are favoured around pH 7 and their stability is enhanced by the macrochelation from another histidyl residue in the mononuclear complexes

  

(see Scheme 1b). Another important consequence of the independence of the histidyl sites comes from the existence of coordination isomers for the mononuclear species of all peptides and for the dinuclear species of HuPrP(84–114). CD spectroscopy was able to distinguish among coordination isomers and the preference for metal binding follows the order of: His111 > His96 > His85 (see Figure 8). A further increase in pH resulted in the deprotonation and metal-ion coordination of the third amide functions at each metal-binding site with the ($N_{im}$,$N^-$,$N^-$,$N^-$)-coordination mode. Spectroscopic measurements made it also clear that the four lysyl amino groups of the peptides are not metal-binding sites in any cases.

The coordination modes of this 31-mer peptide reconfirm those previously proposed modes for the copper(II) binding with HuPrP(57–91)[26] and HuPrP(91–115) peptide fragments.[52] It is worth noting that our results indicate, for the first time, that one of the common coordination modes, namely the macrochelate ring formation, involves the binding of one imidazole nitrogen (His85) from the octarepeat region and two imidazole nitrogen atoms from the unstructured domain (His96 and His111). An additional histidine interaction with $Cu^{2+}$ coordinated to four histidines that are contained in the HuPrP(57–91) octarepeat region has been hypothesised in the full-length protein.[52] Thus, our data support this hypothesis, though we are aware of the limits of our mimic system. In addition, on the basis of the preference of the prion protein for multiple histidine–$Cu^{2+}$ coordination with macrochelate ring formation, it has recently been proposed that this species is likely the highest-affinity form of binding in the protein.[52,53] Based on the comparison between the estimated affinity constants of $Cu^{2+}$–macrochelate complex species and those, previously determined, of the extracellular $Cu^{2+}$ transporters (albumin, ceruloplasmin, amino acids), it has been hypothesised that only a small percentage of prion protein could bind to $Cu^{2+}$ under normal conditions in the central nervous system. The distribution diagram of the ternary system ($Cu^{2+}$–HuPrP(84–114)–AspAlaHis-NHMe)[54] shows that the peptide that simulates the high-affinity $Cu^{2+}$ binding of albumin is able to completely sequester $Cu^{2+}$ when the two ligands and the metal ion are in a 1:1:1 ratio (see Supporting Information). To determine whether PrP is an authentic cuproprotein, we need to know the stability constants of the macrochelate species that is formed with the entire N-terminus region, which encompasses six histidine residues. Thus, the results reported here represent only a first useful basis to rationalise the conclusions that will be presented in a forthcoming publication concerning the entire PrP N terminus polypeptide that was recently synthesised by us as a soluble derivative. Thus, a complete quantitative picture of the $Cu^{2+}$-binding features within the entire N-terminal domain should be obtained, and this should clarify the in vivo role of PrP as a copper protein.

## Experimental Section

**General**: All *N*-fluorenylmethoxycarbonyl (Fmoc)-protected amino acids, (Fmoc-Lys(Boc)-OH, Fmoc-Thr(*t*-Bu)-OH, Fmoc-Asn(Trt)-OH, Fmoc-Met-OH, Fmoc-His(Trt)-OH, Fmoc-Ala-OH, Fmoc-Gly-OH, Fmoc-Ser-(*t*-Bu)-OH, Fmoc-Trp(Boc)-OH, Fmoc-Pro-OH) and Fmoc-Gln(Trt), and 2-(1-*H*-benzotriazole-1-yl)-1,1,3,3-tetramethyluronium tetrafluoroborate (TBTU) were obtained from Novabiochem (Switzerland); Fmoc PAL-PEG resin, *N*,*N*-diisopropylethylamine (DIEA), *N*,*N*-dimethylformamide (DMF, peptide synthesis grade) and 20% piperidine/DMF solution were obtained from Applied Biosystems; *N*-hydroxybenzotriazole (HOBT), triisopropylsilane (TIS), trifluoroacetic acid (TFA), ethandithiol (EDT), were purchased from Sigma–Aldrich. All other chemicals were of the highest available grade and were used without further purification.

Preparative reversed-phase high-performance liquid chromatography (RP-HPLC) was carried out by means of a Varian PrepStar 200 model SD-1 chromatography system equipped with a Prostar photodiode array detector with detection at 222 nm. Purification was performed by eluting with solvent A (0.1% TFA in water) and B (0.1% TFA in acetonitrile) on a Vydac $C_{18}$ 250×22 mm (300 Å pore size, 10–15 μm particle size) column, at flow rate of 20 mL min$^{-1}$. Analytical RP-HPLC analyses were performed by using a Waters 1525 instrument, equipped with a Waters 2996 photodiode array detector with detection at 222 nm.

The peptide samples were analysed by using gradient elution with solvent A and B on a Vydac $C_{18}$ 250×4.6 mm (300 Å pore size, 5 μm particle size) column, run at a flow rate of 1 mL min$^{-1}$.

**Peptide synthesis and purification**: The HuPrP(91–115), HuPrP(84–114), HuPrP(84–114)His85Ala, HuPrP(84–114)His96Ala and HuPrP(84–114)His111Ala peptides were assembled by using the solid-phase peptide synthesis strategy on a Pioneer™ Peptide Synthesiser. All residues were introduced according to TBTU/HOBT/DIEA activation method for Fmoc chemistry on a Fmoc-PAL-PEG resin (substitution: 0.22 mmol g$^{-1}$, 0.33 mmol scale synthesis, 1.5 g of resin). The synthesis was carried out under a fourfold excess of amino acid at every cycle, and each amino acid was recirculated through the resin for 35 min. The removal of the Fmoc protecting group during the synthesis was achieved by means of 20% piperidine solution in DMF. N-Terminal acetylation was performed by treating the fully assembled and protected peptide resins (after removal of the N-terminal Fmoc group) with a solution that contained acetic anhydride (6% *v*/*v*) and DIEA (5% *v*/*v*) in DMF.

The peptides were cleaved off of their respective resins and simultaneously deprotected by treatment with a mixture of TFA/TIS/EDT/$H_2O$ (94.5/1.0/2.5/2.5% v/v) for 2 h at room temperature. Each free peptide-containing solution was filtered off from the resin and concentrated in vacuo at 30 °C. The peptide was precipitated with cold freshly distilled diethyl ether. The precipitate was then filtered, dried under vacuum, redissolved in water and lyophilised. The resulting crude peptides were purified by preparative RP-HPLC.

**AcGlnGlyGlyGlyThrHisSerGlnTrpAsnLysProSerLysProLysThrAsnMetLysHisMetAlaGlyNH$_2$ (HuPrP(91–115))**: From 0 to 8 min, isocratic conditions in 8% B, then a linear gradient from 8 to 16% B over 28 min, finally, isocratic conditions in 16% B from 28 to 32 min. Yield = 56% ($R_t$ = 30.00 min). Analytical RP-HPLC: from 0 to 5 min isocratic conditions in 7% B, then a linear gradient from 7 to 14% B over 25 min, finally isocratic conditions in 14% B from 25 to 30 min ($R_t$ = 29 min); MS: *m*/*z*: 1360.3 $[M+2H]^{2+}$, 907.3 $[M+3H]^{3+}$ (calcd: 2718.32).

**AcProHisGlyGlyGlyTrpGlyGlnGlyGlyGlyThrHisSerGlnTrpAsnLysProSerLysProLysThrAsnMetLysHisMetAlaGlyNH$_2$ (HuPrP(84–114))**: From 0 to 8 min isocratic conditions in 14% B, then a linear gradient from 14 to 19% B over 20 min, finally isocratic conditions in 19% B from 20 to 25 min. Yield = 48% ($R_t$ = 21.6 min). Analytical RP-HPLC: from 0 to 5 min isocratic conditions in 5% B, then linear gradient from 5 to 25% B over 20 min, finally isocratic conditions in 25% B from 20 to 30 min ($R_t$ = 22.6 min); MS: *m*/*z*: 1649.5 $[M+2H]^{2+}$, 1100.7 $[M+3H]^{3+}$, 825.9 $[M+4H]^{4+}$ (calcd: 3295.6).

**AcProAlaGlyGlyGlyTrpGlyGlnGlyGlyGlyThrHisSerGlnTrpAsnLysProSerLysProLysThrAsnMetLysHisMetAlaGlyNH$_2$ (HuPrP(84–114)His85-**

  

**Ala)**: From 0 to 8 min isocratic conditions in 15% B, then a linear gradient from 15 to 20% B over 28 min. Yield = 43% ($R_t$ = 19.23 min). Analytical RP-HPLC: from 0 to 5 min isocratic conditions in 7% B, then a linear gradient from 7 to 20% B over 25 min, finally isocratic conditions in 20% B from 25 to 30 min ($R_t$ = 24 min); MS: *m*/*z*: 1616.5 $[M+2H]^{2+}$, 1078.6 $[M+3H]^{3+}$, 809.6 $[M+4H]^{4+}$ (calcd: 3229.54).

**AcProHisGlyGlyGlyTrpGlyGlnGlyGlyGlyThrAlaSerGlnTrpAsnLysProSerLysProLysThrAsnMetLysHisMetAlaGlyNH$_2$ (HuPrP(84–114)His96Ala)**: From 0 to 8 min isocratic conditions in 15% B, then a linear gradient from 15 to 20% B over 28 min. Yield = 42% ($R_t$ = 18.26 min). Analytical RP-HPLC: from 0 to 5 min isocratic conditions in 7% B, then a linear gradient from 7 to 20% B over 25 min, finally isocratic conditions in 20% B from 25 to 30 min ($R_t$ = 26 min); MS: *m*/*z*: 1616.4 $[M+2H]^{2+}$, 1078.3 $[M+3H]^{3+}$ 809.5 $[M+4H]^{4+}$ (calcd: 3229.54).

**AcProHisGlyGlyGlyTrpGlyGlnGlyGlyGlyThrHisSerGlnTrpAsnLysProSerLysProLysThrAsnMetLysAlaMetAlaGlyNH$_2$ (HuPrP(84–114)His111Ala)**: From 0 to 8 min isocratic conditions in 15% B, then linear gradient from 15 to 20% B over 28 min. Yield = 60% ($R_t$ = 20.00 min). Analytical RP-HPLC: from 0 to 5 min isocratic conditions in 7% B, then linear gradient from 7 to 20% B over 25 min, finally isocratic conditions in 20% B from 25 to 30 min ($R_t$ = 26.5 min); MS: *m*/*z*: 1616.5 $[M+2H]^{2+}$, 1078.4 $[M+3H]^{3+}$, 809.5 $[M+4H]^{4+}$ (calcd: 3229.54).

**pH-Potentiometric measurements**: The pH-potentiometric titrations were performed in 3 cm$^3$ samples at $1\times10^{-3}$ mol dm$^{-3}$ ligand concentration with the metal-to-ligand ratios between 1:1 to 3:1 (for the 2-His peptides) or 4:1 [in the case of HuPrP(84–114)]. During the titration, argon was bubbled through the samples to ensure the absence of oxygen and carbon dioxide. The samples were stirred by a VELP Scientific magnetic stirrer. All pH-potentiometric measurements were carried out at 298 K and at a constant ionic strength of 0.2 M KCl. pH Measurements were made with a MOLSPIN pH-meter equipped with a 6.0234.100 combination glass electrode (Metrohm) and a MOL-ACS microburette controlled by a computer. The recorded pH readings were converted to hydrogen ion concentration as described by Irving et al.[55] The protonation constants of the ligands and overall stability constants ($\log\beta_{pqr}$) of the $Cu^{2+}$ complexes were calculated by means of the general computational programs, PSEQUAD[51] and HYPERQUAD,[36] by using Equations (1) and (2).

$$pM + qH + rL = M_pH_qL_r \quad (1)$$

$$\beta_{pqr} = \frac{[M_pH_qL_r]}{[M]^p\,[H]^q\,[L]^r} \quad (2)$$

**UV/Vis spectroscopy**: Spectroscopic measurements: UV/Vis spectra of the $Cu^{2+}$ complexes were recorded from 250–900 nm on a Hewlett–Packard HP 8453 diode array or a Perkin–Elmer Lambda 25 scanning spectrophotometer in the same concentration range as was used for the pH-potentiometric measurements.

**CD spectroscopy**: CD spectra of the ligands and the $Cu^{2+}$ complexes were recorded on a JASCO J-810 spectropolarimeter by using 1 or 10 mm cells in the 200–800 nm wavelength range at the same concentration as used for pH-potentiometry.

**EPR spectroscopy**: Anisotropic X-band EPR spectra of frozen solutions were recorded at 120 K, by using a Bruker EMX spectrometer after the addition of ethylene glycol to ensure good glass formation. Copper(II) stock solutions for EPR measurements were prepared from $CuSO_4{\cdot}5H_2O$ that had been enriched with $^{63}Cu$ to achieve better resolution of EPR spectra. Metallic copper (99.3% $^{63}Cu$ and 0.7% $^{65}Cu$) was purchased from JV Isoflex, (Moscow, Russia) for this purpose and was converted into the sulfate. Only anisotropic EPR spectra have been measured. In fact, in comparison with isotropic spectra, the former can give information about the symmetry and the coordination geometry of the $Cu^{2+}$ complexes. Moreover, the anisotropic hyperfine-splitting constant shows the greatest sensitivity to the identity of the coordinated donors and finally it is easier to distinguish when more than one species is present in solution. Hyperfine-coupling constant ($A_\parallel$) are expressed in $10^{-4}$ cm$^{-1}$.

**Electrospray ionisation mass spectrometry (ESI-MS) analysis**: ESI-MS spectra were recorded on a Finnigan LCQ-Duo ion trap electrospray mass spectrometer. Peptide solutions were introduced into the ESI source through 100 μm i.d. fused silica, from a 250 μL syringe. The experimental conditions for spectra acquired in positive-ion mode were as follows: needle voltage: 2.5 kV, flow rate: 5 μL min$^{-1}$, source temperature: 150 °C; *m*/*z* range: 200–2000, cone potential: 46 V, tube lens offset: 16 V.

The metal-complex solutions were prepared by dissolving the peptide and $CuSO_4{\cdot}5H_2O$ in Milli-Q water at a 1:1 ligand-to-metal ratio (ligand concentration ranging from $1\times10^{-5}$ to $5\times10^{-5}$ mol·dm$^{-3}$) and were investigated in the 5.0–10.0 pH range; the pH values were adjusted by adding HCl or NaOH to the solutions.

## Acknowledgements

This work was supported by MTA(Hungary)-CNR(Italy) bilateral program and by MIUR Grants 196 D.M 1105/2002, PRIN 2005035582, FIRB RBNE03PX83, OTKA T048352, D048488 and PAL-18657/2005.

[1] S. B. Prusiner, *Proc. Natl. Acad. Sci. USA* **1998**, *95*, 13363–13383.
[2] J. Collinge, *Annu. Rev. Neurosci.* **2001**, *24*, 519–550.
[3] S. B. Prusiner, *Science* **1982**, *216*, 136–144.
[4] R. Zahn, *J. Mol. Biol.* **2003**, *334*, 477–488.
[5] R. Riek, S. Hornemann, G. Wider, M. Billeter, R. Glockshuber, K. Wüthrich, *Nature* **1996**, *382*, 180–182.
[6] N. Stahl, D. R. Borchelt, K. Hsiao, S. B. Prusiner, *Cell* **1987**, *51*, 229–240.
[7] H. Büeler, M. Fischer, Y. Lang, H. Bluethmann, H. P. Lipp, S. J. Dearmond, S. B. Prusiner, M. Aguet, C. Weissmann, *Nature* **1992**, *356*, 577–582.
[8] J. Collinge, M. A. Whittington, K. C. L. Sidle, C. J. Smith, M. S. Palmer, A. R. Clarke, J. G. R. Jefferys, *Nature* **1994**, *370*, 295–297.
[9] D. R. Brown, K. Qin, J. W. Herms, A. Madlung, J. Manson, R. Strome, P. E. Fraser, T. Kruck, A. von Bohlen, W. Schulz-Schaeffer, A. Giese, D. Westaway, H. Kretzschmar, *Nature* **1997**, *390*, 684–687.
[10] M. P. Hornshaw, J. R. McDermott, J. M. Candy, *Biochem. Biophys. Res. Commun.* **1995**, *207*, 621–629.
[11] M. P. Hornshaw, J. R. McDermott, J. M. Candy, J. H. Lakey, *Biochem. Biophys. Res. Commun.* **1995**, *214*, 993–999.
[12] G. S. Jackson, I. Murray, L. L. P. Hosszu, N. Gibbs, J. P. Waltho, A. R. Clarke, J. Collinge, *Proc. Natl. Acad. Sci. USA* **2001**, *98*, 8531–8535.
[13] T. Miura, A. Hori-i, H. Mototani, H. Takeuchi, *Biochemistry* **1999**, *38*, 11560–11569.
[14] J. H. Viles, F. E. Cohen, S. B. Prusiner, D. B. Goodin, P. E. Wright, H. J. Dyson, *Proc. Natl. Acad. Sci. USA* **1999**, *96*, 2042–2047.
[15] R. M. Whittal, H. L. Ball, F. E. Cohen, A. L. Burlingame, S. B. Prusiner, M. A. Baldwin, *Protein Sci.* **2000**, *9*, 332–343.
[16] C. S. Burns, E. Aronoff-Spencer, C. M. Dunham, P. Lario, N. I. Avdievich, W. E. Antholine, M. M. Olmstead, A. Vrielink, G. J. Gerfen, J. Peisach, W. G. Scott, G. L. Millhauser, *Biochemistry* **2002**, *41*, 3991–4001.
[17] A. P. Garnett, J. H. Viles, *J. Biol. Chem.* **2003**, *278*, 6795–6802.
[18] E. Aronoff-Spencer, C. S. Burns, N. I. Avdievich, G. J. Gerfen, J. Peisach, W. E. Antholine, H. L. Ball, F. E. Cohen, S. B. Prusiner, G. L. Millhauser, *Biochemistry* **2000**, *39*, 13760–13771.
[19] C. S. Burns, E. Aronoff-Spencer, G. Legname, S. B. Prusiner, W. E. Antholine, G. J. Gerfen, J. Peisach, G. L. Millhauser, *Biochemistry* **2003**, *42*, 6794–6803.
[20] J. Stöckel, J. Safar, A. C. Wallace, F. E. Cohen, S. B. Prusiner, *Biochemistry* **1998**, *37*, 7185–7193.
[21] M. L. Kramer, H. D. Kratzin, B. Schmidt, A. Römer, O. Windl, S. Liemann, S. Hornemann, H. Kretzschmar, *J. Biol. Chem.* **2001**, *276*, 16711–16719.

  

[22] R. P. Bonomo, G. Impellizzeri, G. Pappalardo, E. Rizzarelli, G. Tabbì, *Chem. Eur. J.* **2000**, *6*, 4195–4202.
[23] R. P. Bonomo, V. Cucinotta, A. Giuffrida, G. Impellizzeri, A. Magrì, G. Pappalardo, E. Rizzarelli, A. M. Santoro, G. Tabbì, L. I. Vagliasindi, *Dalton Trans.* **2005**, 150–158.
[24] S. Morante, R. Gonzalez-Iglesias, C. Potrich, C. Meneghini, W. Meyer-Klaucke, G. Menestrina, M. Gasset, *J. Biol. Chem.* **2004**, *279*, 11753–11759.
[25] D. Valensin, M. Luczkowski, F. M. Mancini, A. Legowska, E. Gaggelli, G. Valensin, K. Rolka, H. Kozlowski, *Dalton Trans.* **2004**, 1284–1293.
[26] M. Chattopadhyay, E. D. Walter, D. J. Newell, P. J. Jackson, E. Aronoff-Spencer, J. Peisach, G. J. Gerfen, B. Bennett, W. E. Antholine, G. L. Millhauser, *J. Am. Chem. Soc.* **2005**, *127*, 12647–12656.
[27] C. E. Jones, S. R. Abdelraheim, D. R. Brown, J. H. Viles, *J. Biol. Chem.* **2004**, *279*, 32018–32027.
[28] C. E. Jones, M. Klewpatinond, S. R. Abdelraheim, D. R. Brown, J. H. Viles, *J. Mol. Biol.* **2005**, *346*, 1393–1407.
[29] G. Di Natale, G. Grasso, G. Impellizzeri, D. La Mendola, G. Micera, N. Mihala, Z. Nagy, K. Ősz, G. Pappalardo, V. Rigó, E. Rizzarelli, D. Sanna, I. Sóvágó, *Inorg. Chem.* **2005**, *44*, 7214–7225.
[30] A. R. Thompsett, S. R. Abdelraheim, M. Daniels, D. R. Brown, *J. Biol. Chem.* **2005**, *280*, 42750–42758.
[31] S. S. Hasnain, L. M. Murphy, R. W. Strange, J. G. Grossmann, A. R. Clarke, G. S. Jackson, J. Collinge, *J. Mol. Biol.* **2001**, *311*, 467–473.
[32] M. F. Jobling, X. Huang, L. R. Stewart, K. J. Barnham, C. Curtain, I. Volitakis, M. Perugini, A. R. White, R. A. Cherny, C. L. Masters, C. J. Barrow, S. J. Collins, A. I. Bush, R. Cappai, *Biochemistry* **2001**, *40*, 8073–8084.
[33] B. Belosi, E. Gaggelli, R. Guerrini, H. Kozlowski, M. Luczkowski, F. M. Mancini, M. Remelli, D. Valensin, G. Valensin, *ChemBioChem* **2004**, *5*, 349–359.
[34] V. Jószai, Z. Nagy, K. Ősz, D. Sanna, G. Di Natale, D. La Mendola, G. Pappalardo, E. Rizzarelli, I. Sóvágó, *J. Inorg. Biochem.* **2006**, *100*, 1399–1409.
[35] D. Grasso, G. Grasso, V. Guantieri, G. Impellizzeri, C. La Rosa, D. Milardi, G. Micera, K. Ősz, G. Pappalardo, E. Rizzarelli, D. Sanna, I. Sóvágó, *Chem. Eur J.* **2006**, *12*, 537–547.
[36] P. Gans, A. Sabatini, A. Vacca, *Talanta* **1996**, *43*, 1739–1753.
[37] E. Gaggelli, H. Kozlowski, D. Valensin, G. Valensin, *Chem. Rev.* **2006**, *106*, 1995–2044.
[38] M. Luczkowski, H. Kozlowski, M. Stawikowski, K. Rolka, E. Gaggelli, D. Valensin, G. Valensin, *J. Chem. Soc. Dalton Trans.* **2002**, 2269–2274.
[39] D. R. Brown, H. Kozlowski, *Dalton Trans.* **2004**, 1907–1917.
[40] H. Kozlowski, W. Bal, M. Dyba, T. Kowalik-Jankowska, *Coord. Chem. Rev.* **1999**, *184*, 319–346.
[41] D. Sanna, G. Micera, C. Kállay, V. Rigó, I. Sóvágó, *Dalton Trans.* **2004**, 2702–2707.
[42] C. Kállay, K. Várnagy, G. Malandrinos, N. Hadjiliadis, D. Sanna, I. Sóvágó, *Dalton Trans.* **2006**, 4545–4552.
[43] M. Casolaro, M. Chelli, M. Ginanneschi, F. Laschi, L. Messori, M. Muniz-Miranda, A. M. Papini, T. Kowalik-Jankowska, H. Kozlowski, *J. Inorg. Biochem.* **2002**, *89*, 181–190.
[44] J. Brasun, C. Gabbiani, M. Ginanneschi, L. Messori, M. Orfei, J. Swiatek-Kozlowska, *J. Inorg. Biochem.* **2004**, *98*, 2016–2021.
[45] B. Bóka, A. Myari, I. Sóvágó, N. Hadjiliadis, *J. Inorg. Biochem.* **2004**, *98*, 113–122.
[46] M. Luczkowski, K. Wisniewska, L. Lankiewicz, H. Kozlowski, *J. Chem. Soc. Dalton Trans.* **2002**, 2266–2268.
[47] M. Remelli, M. Luczkowski, A. M. Bonna, Z. Mackiewicz, C. Conato, H. Kozlowski, *New J. Chem.* **2003**, *27*, 245–250.
[48] R. P. Bonomo, L. Casella, L. De Gioia, H. Molinari, G. Impellizzeri, T. Jordan, G. Pappalardo, R. Purrello, E. Rizzarelli, *J. Chem. Soc. Dalton Trans.* **1997**, 2387–2389.
[49] G. Pappalardo, G. Impellizzeri, R. P. Bonomo, T. Campagna, G. Grasso, M. G. Saita, *New J. Chem.* **2002**, *26*, 593–600.
[50] A. Jancsó, Z. Paksi, N. Jakab, B. Gyurcsik, A. Rockenbauer, T. Gajda, *Dalton Trans.* **2005**, 3187–3194.
[51] L. Zékány, I. Nagypál, in *Computational Methods for the Determination of Stability Constants* (Ed.:D. J. Leggett), Plenum, New York, **1985**, pp. 291–355.
[52] M. A. Wells, C. Jelinska, L. L. P. Hosszu, C. J. Craven, A. R. Clarke, J. Collinge, J. P. Waltho, G. S. Jackson, *Biochem. J.* **2006**, *400*, 501–510.
[53] M. A. Wells, G. S. Jackson, S. Jones, L. L. P. Hosszu, C. J. Craven, A. R. Clarke, J. Collinge, J. P. Waltho, *Biochem. J.* **2006**, *399*, 435–444.
[54] G. Arena, E. Rizzarelli, B. Sarkar, *Inorg. Chim. Acta* **1979**, *37*, L555–L557.
[55] H. Irving, G. Miles, L. D. Pettit, *Anal. Chim. Acta* **1967**, *38*, 475–488.

Received: November 2, 2006
Revised: March 27, 2007
Published online: June 13, 2007

  